FIRST-YEAR SLOAN DIGITAL SKY SURVEY-II (SDSS-II) SUPERNOVA RESULTS: CONSTRAINTS ON NON-STANDARD COSMOLOGICAL MODELS

J. Sollerman[1,2], E. Mörtsell[3], T. M. Davis[1,4], M. Blomqvist[2], B. Bassett[5,6], A. C. Becker[7], D. Cinabro[8], A. V. Filippenko[9], R. J. Foley[9,10,11], J. Frieman[12,13,14], P. Garnavich[15], H. Lampeitl[16], J. Marriner[14], R. Miquel[17,18], R. C. Nichol[16], M. W. Richmond[19], M. Sako[20], D. P. Schneider[21], M. Smith[5,6,16], J. T. Vanderplas[7], and J. C. Wheeler[22]

Draft version September 1, 2009

ABSTRACT

We use the new Type Ia supernovae (SNe Ia) discovered by the Sloan Digital Sky Survey-II Supernova Survey together with additional supernova datasets as well as observations of the cosmic microwave background and baryon acoustic oscillations to constrain cosmological models. This complements the standard cosmology analysis presented by Kessler et al. (2009) in that we discuss and rank a number of the most popular non-standard cosmology scenarios. When this combined dataset is analyzed using the MLCS2k2 light-curve fitter, we find that more exotic models for cosmic acceleration provide a better fit to the data than the ΛCDM model. For example, the flat Dvali-Gabadadze-Porrati model is ranked higher by our information-criteria tests than the standard model with a flat universe and a cosmological constant. When the supernova dataset is instead analyzed using the SALT-II light-curve fitter, the standard cosmological-constant model fares best. This investigation of how sensitive cosmological model selection is to assumptions about, and within, the light-curve fitters thereby highlights the need for an improved understanding of these unresolved systematic effects. Our investigation also includes inhomogeneous Lemaître-Tolman-Bondi (LTB) models. While our LTB models can be made to fit the supernova data as well as any other model, the extra parameters they require are not supported by our information-criteria analysis. Finally, we explore more model-independent ways to investigate the cosmic expansion based on this new dataset.

Subject headings: cosmology: observations — supernovae : general

[1] Dark Cosmology Centre, Niels Bohr Institute, University of Copenhagen, Juliane Maries Vej 30, Copenhagen, Denmark.
[2] The Oskar Klein Centre, Department of Astronomy, AlbaNova, Stockholm University, 106 91 Stockholm, Sweden.
[3] The Oskar Klein Centre, Department of Physics, AlbaNova, Stockholm University, 106 91 Stockholm, Sweden.
[4] School of Mathematics and Physics, University of Queensland, QLD, 4072, Australia.
[5] South African Astronomical Observatory, P.O. Box 9, Observatory 7935, South Africa.
[6] Department of Mathematics and Applied Mathematics, University of Cape Town, Rondebosch 7701, South Africa.
[7] Department of Astronomy, University of Washington, Box 351580, Seattle, WA 98195.
[8] Department of Physics, Wayne State University, Detroit, MI 48202.
[9] Department of Astronomy, University of California, Berkeley, CA 94720-3411.
[10] Harvard-Smithsonian Center for Astrophysics, 60 Garden Street, Cambridge, MA 02138.
[11] Clay Fellow.
[12] Kavli Institute for Cosmological Physics, The University of Chicago, 5640 South Ellis Avenue Chicago, IL 60637.
[13] Department of Astronomy and Astrophysics, The University of Chicago, 5640 South Ellis Avenue Chicago, IL 60637.
[14] Center for Astrophysics, Fermi National Accelerator Laboratory, P. O. Box 500, Batavia IL 60510.
[15] University of Notre Dame, 225 Nieuwland Science, Notre Dame, IN 46556-5670.
[16] Institute of Cosmology and Gravitation, University Portsmouth, Portsmouth, PO1 3FX, UK.
[17] Institució Catalana de Recerca i Estudis Avançats, Barcelona, Spain.
[18] Institut de Física d'Altes Energies, E-08193 Bellaterra, Barcelona, Spain.
[19] Physics Department, Rochester Institute of Technology, Rochester, NY 14623.
[20] Department of Physics and Astronomy, University of Pennsylvania, 209 South 33rd Street, Philadelphia, PA 19104.
[21] Department of Astronomy and Astrophysics, 525 Davey Laboratory, Pennsylvania State University, University Park, PA 16802.
[22] Department of Astronomy, University of Texas, Austin, TX 78712.

1. INTRODUCTION

The Type Ia supernova (SN Ia) measurements which first indicated an accelerating expansion of the universe (Riess et al. 1998; Perlmutter et al. 1999; see Filippenko 2005 for a review) have been confirmed and substantiated by a second generation of high-redshift supernova experiments (Riess et al. 2004; Astier et al. 2006; Wood-Vasey et al. 2007; Riess et al. 2007). An important step forward in this respect was recently taken with the Sloan Digital Sky Survey-II (SDSS-II) Supernova Survey (Frieman et al. 2008). This three-year survey, undertaken with a large CCD camera on a dedicated 2.5-m telescope in New Mexico (Gunn et al. 2006), has discovered and followed several hundred SNe Ia, mainly in the redshift interval $z = [0.01, 0.45]$. These intermediate redshifts were previously underexplored, and filling this "redshift desert" not only provides important new constraints on cosmology (Kessler et al. 2009), but will also help constrain systematic effects by bridging the low-z and the high-z supernova populations.

The first-year SDSS supernova dataset is discussed in three companion papers, including this one. Kessler et al. (2009, hereafter K09) present the dataset in detail and also use it to constrain standard cosmological models. Lampeitl et al. (2009) combine the SDSS SN data with other constraints to derive joint constraints on

dark energy from low-redshift ($z < 0.4$) measurements only; they also explore the consistency of the SN and BAO distance scales.

To complement and extend the cosmological analysis presented in these papers we will in this paper use the first-year SDSS-II supernova data to explore several alternative cosmological models. Following the analysis outlined by Davis et al. (2007, hereafter D07), we combine the 103 new SDSS-II SNe Ia in the K09 dataset with new analyses of previously available SN Ia datasets, as well as complementary data, to explore non-standard cosmologies. We also investigate the use of more model-free approaches in constraining the evolution of the universe.

This paper is organized as follows. In Section 2 we describe the datasets invoked in the analysis and how they are combined, while in Section 3 we present the cosmological models that are investigated in this work. In Section 4 we discuss our results. Section 5 includes a discussion of systematic effects, while Section 6 presents some ways of expressing generalized parameters from the supernova dataset. Finally, in Section 7 we provide a summary of our results.

When we refer to the "standard model" we mean Friedmann-Robertson-Walker cosmology with a constant dark energy equation-of-state parameter, also known as "w Cold Dark Matter" (wCDM), of which the cosmological-constant model (ΛCDM) is a special case. We use units in which $c = 1$.

2. DATASETS

In this paper we make use of constraints from several different datasets in order to test a number of cosmological models. Compared to the previous analysis by D07, here we make use of an enlarged and re-analyzed supernova set, a new prescription as well as new data for the baryonic acoustic oscillations (BAO), and also an updated cosmic microwave background (CMB) analysis. In this section we present these datasets, and describe how they are combined.

2.1. Type Ia Supernovae

The primary new dataset used in this analysis comprises the 103 new SNe Ia from the first-year SDSS-II supernova survey (Frieman et al. 2008; Sako et al. 2008; K09).

This sample is published and discussed at length in our companion paper (K09) which also includes a comprehensive and consistent re-analysis of other sets of local and high-z SNe Ia, using the same light-curve fitter. This is important since it ensures that all the supernova datasets are treated in a uniform manner regarding selection criteria and light-curve fitting. For the analysis presented in this paper we start by discussing the supernova dataset analyzed using the Multicolor Light Curve Shape 2k2 fitter: (MLCS; Jha et al. 2007)[23]. According to the MLCS analysis of K09, the standard ΛCDM cosmological model provides a rather poor fit to these data. We will also discuss calculations for the K09 SN dataset analyzed with the SALT-II light-curve fitter (Guy et al. 2007),

---

[23] We have used the entire Nearby+SDSS+ESSENCE+SNLS+HST dataset (e) of K09; http://das.sdss.org/va/SNcosmology/sncosm09_fits.tar.gz.

---

which is better fit by the ΛCDM concordance model. In total, we use 288 SNe from the analysis of K09. The distance moduli and redshifts for these SNe are provided in K09 (their Table 10 for MLCS and Table 14 for SALT-II). The very detailed and restrictive selection criteria for the total sample of SNe are described in K09; following their analysis we have used only supernovae with $z > 0.02$ and added an additional "intrinsic" dispersion of $\sigma_{\rm add} = 0.16$ mag to the uncertainties output by the light-curve fitter. Since this added dispersion is motivated in K09 to make the *local* MLCS SN Hubble diagram have a χ^2 equal to unity per degree of freedom, it is essentially independent of cosmology. A similar intrinsic dispersion (we use 0.14 mag) gives a $\chi^2_{\rm d.o.f.}=1$ for the global SALT-II fit. Our supernova dataset is thus a well-selected sample compiled from many surveys (Kessler et al. 2009; Wood-Vasey et al. 2007; Astier et al. 2006; Riess et al. 2007; Jha et al. 2007, and references therein).

2.2. Cosmic Microwave Background

When analyzing CMB observations there are two useful parameters commonly employed. One describes the scaled distance to recombination, $\mathcal{R}$, and the other the angular scale of the sound horizon at recombination, ℓ_A (e.g., Komatsu et al. 2009; Elgarøy & Multamäki 2007; Wang & Mukherjee 2006).

The shift parameter, $\mathcal{R}$, is given by

$$\mathcal{R} = \sqrt{\frac{\Omega_m}{|\Omega_k|}} S_k \left[\sqrt{|\Omega_k|} \int_0^{z_*} \frac{H_0 \, dz}{H(z)} \right], \qquad (1)$$

where $S_k(x) = \sin x, x, \sinh x$ for $k = 1, 0, -1$, respectively, and z_* is the redshift of the last-scattering surface.

The position of the first CMB power-spectrum peak, which represents the angular scale of the sound horizon at recombination, is given by

$$\ell_A = \pi \frac{d_{\rm A}(z_*)}{r_{\rm s}(z_*)}, \qquad (2)$$

where $d_{\rm A}(z_*)$ is the comoving angular-diameter distance to recombination while the comoving sound horizon at photon decoupling, $r_{\rm s}$, is given by

$$r_{\rm s} = \int_{z_*}^{\infty} \frac{c_s}{H(z)} dz, \qquad (3)$$

which depends upon the speed of sound before recombination, c_s. Using both these parameters in combination reproduces closely the fit from the full CMB power spectrum (but see also Elgarøy & Multamäki 2007, for some caveats), and within the standard model the two parameters are only weakly correlated. Here we use the recent CMB measurements from the five-year Wilkinson Microwave Anisotropy Probe (WMAP) observations, and adopt the values $\ell_A = 302.10 \pm 0.86$ and $\mathcal{R} = 1.710 \pm 0.019$ with correlation coefficient 0.1109 from Komatsu et al. (2009). We further assume $z_* = 1090$ exactly (Komatsu et al. 2009; variations within the uncertainties about this value do not give significant differences in the results).

In a previous paper (D07), we used only the CMB-$\mathcal{R}$ parameter to constrain cosmologies. The same method is used in the K09 paper. Here we will, for reasons outlined below, adopt a different approach.

Although $\mathcal{R}$ has been commonly used to constrain nonstandard models, this approach may not always be entirely appropriate, because parameters close to standard wCDM were assumed in deriving the value of $\mathcal{R}$ (see, e.g., Section 5.4.1 of Komatsu et al. 2009; Kowalski et al. 2008, Section 6). We will therefore use $\mathcal{R}$ *only* for the wCDM model for which it was derived. The resulting fit is of interest because it can reveal any tension between the BAO/CMB and the supernova constraints. As will be further discussed below, ΛCDM is not a good fit to the data when MLCS is used for the SN analysis, and this motivates our search for better fits among non-standard models.

We therefore instead perform an analysis without $\mathcal{R}$ for all the models. In doing this, we use only the product of the acoustic scale ℓ_A with the position of the BAO peak (Section 2.3) to complement the SN data.

2.3. Baryon Acoustic Oscillations

As with the CMB, there are several parameters in common use for comparing BAO observations to theoretical models. The most immediately observable of these is a measurement of the ratio of the sound horizon scale at the drag epoch, $r_s(z_d)$, to the dilation scale, $D_V(z)$. The drag epoch, $z_d \approx 1020$, is the epoch at which the acoustic oscillations are frozen in.

A more model-independent constraint can be achieved by multiplying the BAO measurement of $r_s(z_d)/D_V(z)$ with the CMB measurement $\ell_A = \pi d_A(z_*)/r_s(z_*)$, thus cancelling some of the dependence on the sound horizon scale.

Percival et al. (2009) measured $r_s(z_d)/D_V(z)$ at two redshifts, $z = 0.2$ and $z = 0.35$, finding $r_s(z_d)/D_V(0.2) = 0.1905 \pm 0.0061$ and $r_s(z_d)/D_V(0.35) = 0.1097 \pm 0.0036$. Combining this with ℓ_A gives the combined BAO/CMB-ℓ_A constraints:

$$\frac{d_A(z_*)}{D_V(0.2)}\frac{r_s(z_d)}{r_s(z_*)} = 18.32 \pm 0.59, \quad (4)$$

$$\frac{d_A(z_*)}{D_V(0.35)}\frac{r_s(z_d)}{r_s(z_*)} = 10.55 \pm 0.35.$$

This combination is equivalent to the S_k/D_V combination used in Percival et al. (2007), but with the ratio of the sound horizon at the two epochs made explicit. Before matching to cosmological models we also need to implement the correction for the difference between the sound horizon at the end of the drag epoch, $z_d \approx 1020$, and the sound horizon at last-scattering, $z_* \approx 1090$. The first is relevant for the BAO, the second for the CMB, and $r_s(z_d)/r_s(z_*) = 1.044 \pm 0.019$ (using values from Komatsu et al. 2009). Inserting this into Equation 4 gives the final constraints we use for the cosmology analysis:

$$\frac{d_A(z_*)}{D_V(0.2)} = 17.55 \pm 0.65, \quad (5)$$

$$\frac{d_A(z_*)}{D_V(0.35)} = 10.10 \pm 0.38.$$

We take into account the correlation between these measurements using the correlation coefficient of 0.337 calculated by Percival et al. (2009).
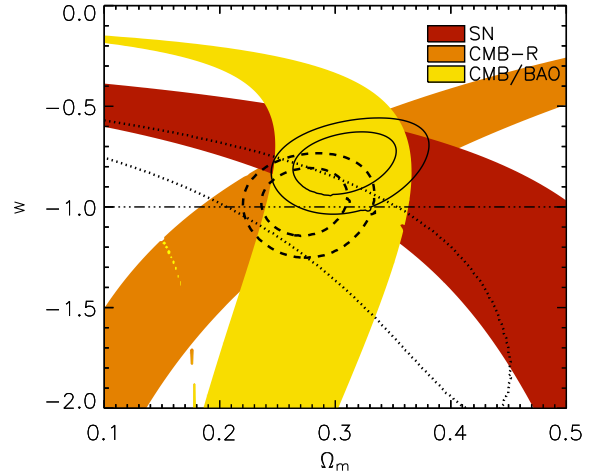

FIG. 1.— Flat dark-energy model (Fw): a flat universe with constant w. The constraint from each of the observational probes is shown by shaded contours. These are all 95% confidence intervals for two parameters. Overlaid with black lines (95% and 99.9% confidence intervals) are contours from combining CMB/BAO-ℓ_A, CMB-$\mathcal{R}$ and SN constraints. The shaded contour labeled SN is for the analysis using the MLCS light-curve fitter. In this plot we have also added the CMB-$\mathcal{R}$ constraints, although these are not included in the model selection. The dotted supernova contours are using the SALT-II fits. For the SALT-II dataset the combined contours are given by the dashed contours, and are clearly in better agreement with the cosmological-constant value, $w = -1$, shown by the dashed-dotted line.

The ratio of sound horizon distances between drag epoch and last-scattering was calculated using the FΛ model (see Table 1) for the evolution between those two redshifts. We expect this to be a good approximation for all the models we test here because the redshift difference between the decoupling and the drag epoch is relatively small, and the sound horizon at decoupling and drag is mostly governed by the fractional difference between the number of photons and baryons.

2.4. Combining the Datasets

To clarify how we combine the data, we show in Figure 1 our best fit to the data in the $w-\Omega_m$ plane for a flat universe with constant w (The Fw model, see Table 1). The constraints from each of the observational probes are shown by contours (according to the figure legend). In this and in all similar figures, these are 95% confidence intervals for two parameters. The supernova dataset fitted with MLCS is shown by the shaded (red) contours, while the SALT-II SN analysis is shown by the dotted contours. The combined contours (95% and 99.9% confidence intervals) are overlaid in black for MLCS and by the dashed contours for SALT-II. In our calculations, we are marginalizing over a common magnitude shift for all SNe, thus allowing for arbitrary values of the Hubble constant, H_0, and the typical absolute magnitude of SNe Ia.

This standard cosmology case is the only one for which we also show the CMB-$\mathcal{R}$ constraint. The constraints from the prescription for the BAO that we have implemented, which also include the CMB-ℓ_A parameter, are labeled CMB/BAO in the figures. Using this CMB/BAO product cancels out some of the dependence on the sound horizon size at last scattering. This thereby removes the

dependence on much of the complex pre-recombination physics that is needed to determine that horizon scale.

In Figure 1, the likelihood analysis takes into account the correlation between ℓ_A and $\mathcal{R}$. In other words, our likelihood plot shows contours derived from CMB-$\mathcal{R}$ separate from contours derived from BAO/CMB-ℓ_A that are then combined taking the weak correlation into account. For the other models, and for the model selection, the CMB-$\mathcal{R}$ is not included. It is then the combination of BAO/CMB-ℓ_A with SN data that we use as the basis for the model comparison performed in this paper. This new analysis is more model independent, and therefore better suited for ranking exotic models. Excluding the $\mathcal{R}$ constraint also leaves more room for models with non-zero curvature.

It was noted by Percival et al. (2007) that the distance between the two BAO redshift bins seemed to be in slight conflict with the supernova measurements for the standard model. Compared to the Percival et al. (2007) BAO/CMB constraints this tension was exacerbated by our new MLCS SN dataset. The new BAO data ease some of this tension (see also Percival et al. 2009; Lampeitl et al. 2009). Rather than selecting only one of the BAO redshift measurements, or any one of the SN light-curve fitters for that matter, we choose to explore the implications of such tension for the more exotic models of interest in this paper.

Figure 1 also helps us understand in a more quantitative way how the different datasets constrain the cosmology. The combined fit using MLCS for the SNe (the SALT-II case will be discussed further in Section 4.3) and also CMB-$\mathcal{R}$ gives $w = -0.79 \pm 0.13$, while the more general method we employ for all models in this paper (omitting $\mathcal{R}$) gives a best fit at $w = -0.83 \pm 0.24$. The error bars quoted are 95% confidence level for one parameter, and we only consider statistical errors. For the approach used by K09 (SN+CMB-$\mathcal{R}$+BAO-A) we find $w = -0.78 \pm 0.13$. Although the procedure we have chosen to combine the different observational constraints also affects the results, it is clear that it is the MLCS analysis of the supernova dataset that makes the main difference in pushing w away from the cosmological-constant value of $w = -1$. We therefore move on to explore more exotic cosmological alternatives.

3. TESTING NON-STANDARD MODELS

Kessler et al. (2009) introduced the first-year SDSS-II SNe to supplement existing data in order to constrain the standard cosmological model. They concentrated on testing a cosmological-constant model and a flat universe model with constant equation-of-state parameter. Here we will extend that analysis to a more general investigation including several of the most popular non-standard models. The models are briefly presented below.

3.1. Beyond-Einstein Models

There are many specific models based on new fundamental physics that make predictions for the expansion history of the universe. We follow D07 in using information criteria to rank these models; see also the recent investigations by, e.g., Kurek & Szydłowski (2008) and Rubin et al. (2009).

With the new SDSS-II supernova data and updated data on the first-peak position of the CMB, combined

TABLE 1
SUMMARY OF MODELS

Model	Abbrev.	Parameters[a]
Flat cosmo. const.	FΛ	Ω_m
Cosmological const.	Λ	Ω_m, Ω_k
Flat constant w	Fw	Ω_m, w
Constant w	w	Ω_m, Ω_k, w
Flat $w(a)$	Fwa	Ω_m, w_0, w_a
Cardassian	Ca	Ω_m, q, n
Flat Chaplygin	FCh	A
Chaplygin	Ch	Ω_k, A
Flat Gen. Chaplygin	FGCh	A, α
Gen. Chaplygin	GCh	Ω_k, A, α
DGP	DGP	Ω_k, Ω_{r_c}
Flat DGP	FDGP	Ω_{r_c}
LTB Gauss	LTBg	$\Omega_{\rm in}$, $\Omega_{\rm out}$, r_0
LTB Sharp	LTBs	$\Omega_{\rm in}$, $\Omega_{\rm out}$, r_0

[a] The free parameters in each model. When fitting the SN Ia data we also fit an additional parameter, $\mathcal{M}$, for the normalization of SN magnitudes. We include this in the number of degrees of freedom and in the number of free parameters considered when calculating information criteria, but do not list it here as a parameter in each model. For more details of these models and the parameters, see D07.

with the new approach to the BAO constraints, we show below that it is worthwhile retesting the non-standard cosmological models examined by Davis et al. (2007).

The selected models include both exotic dark-energy models as well as alternative models that can be interpreted in terms of modifying the theory of gravity. The first class of models we test are the standard cosmological constant, constant w, and variable w models. We also include Dvali-Gabadadze-Porrati (DGP), Cardassian expansion, and several versions of Chaplygin gas models. The appropriate references and the equations we use for describing $H(z)$ in each of these models were collected by Davis et al. (2007, Equations 7–18), and we refer the reader to that paper for further information. For reference, in Table 1 we list all the different models included in this study.

3.2. The Lemaître-Tolman-Bondi Models

In addition to the above models, we also test some inhomogeneous cosmologies. Such models have gathered significant interest in recent years as a means to explain the cosmological observations without invoking dark energy. In the simplest class of such models we live close to the center of a large, spherically symmetric void described by the Lemaître-Tolman-Bondi (LTB) metric (Lemaître 1933, 1997; Tolman 1934; Bondi 1947). The apparent acceleration of the expansion is then caused by the spatial gradients in the metric, such that our local region has a larger Hubble parameter than the outer region. While the LTB models challenge the Copernican principle, several studies have shown that they cannot be ruled out by present observational constraints (e.g., Alnes et al. 2006; Enqvist & Mattsson 2007; Garcia-Bellido & Haugbølle 2008; Caldwell & Stebbins 2008).

The LTB models are characterized by two arbitrary functions, often expressed as the expansion rate $H(r,t)$ and the matter density parameter $\Omega_{\rm M}(r,t)$, which de-

pend not only on time, but also on the radial coordinate. As a consequence, inhomogeneities arise independently in the matter distribution and in the expansion rate.

We will consider LTB models constrained by the requirement that the Big Bang occurred simultaneously throughout space by implementing a particular choice of $H_0(r)$,

$$H_0(r) = \frac{3H_0}{2}\left[\frac{1}{\Omega_k(r)} - \frac{\Omega_M(r)}{\sqrt{\Omega_k^3(r)}}\sinh^{-1}\sqrt{\frac{\Omega_k(r)}{\Omega_M(r)}}\right], \quad (6)$$

so that the time of the Big Bang was $t_{BB} = \frac{2}{3}H_0^{-1}$ for all observers irrespective of their position in space. The model is then completely specified by only one free function, the matter density parameter $\Omega_M(r)$, with $\Omega_M(r) + \Omega_k(r) = 1$. We consider two different density profiles. In the first model, $\Omega_M(r)$ takes the form of a Gaussian underdensity,

$$\Omega_M(r) = \Omega_{out} + (\Omega_{in} - \Omega_{out})e^{-(r/r_0)^2} . \quad (7)$$

This model has three free parameters, where Ω_{in} is the matter density at the center of the void, Ω_{out} is the asymptotic value of the matter density, and r_0 is the scale size of the underdensity.

In the second model, $\Omega_M(r)$ has a much sharper transition from the local to the asymptotic value,

$$\Omega_M(r) = \Omega_{out} + (\Omega_{in} - \Omega_{out})\left(\frac{1 + e^{-r_0/\Delta r}}{1 + e^{(r-r_0)/\Delta r}}\right) . \quad (8)$$

Here r_0 characterizes the size at which the transition occurs and the extra parameter Δr characterizes the transition width. In the limit where Δr goes to zero, the density profile becomes a step function. The two models are designated LTBg and LTBs in Table 1.

Our sharp LTBs model is equivalent to the constrained model in Garcia-Bellido & Haugbølle (2008). We fix the transition width to be $\Delta r = 0.065$ Gpc h^{-1} to obtain a sharp transition, so this is not a free parameter in our model. Furthermore, in both our LTB models we allow Ω_{in} and Ω_{out} to take any positive values ≤ 1, i.e., the models need not be asymptotically flat and in principle we allow also for solutions with a local *overdensity*.

4. RESULTS

4.1. *Model Ranking Using the MLCS Analysis*

The results of all our fits using the MLCS-fit SNe and the combined CMB/BAO constraints are summarized in Table 2. The corresponding results for the SALT-II-fit SNe are presented in Section 4.3. The results are stated in terms of χ^2 and the given degrees of freedom, as goodness of fit (GoF), and in terms of information-criteria (IC) assessments.

The background for the use of IC for these models was reviewed by Davis et al. (2007, their Section 2). We follow their approach (see also Liddle 2004) and use two IC to select the best-fit models. These are the Bayesian information criterion (BIC)

$$\mathrm{BIC} = -2\ln\mathcal{L} + k\ln N, \quad (9)$$

and the Akaike information criterion (AIC)

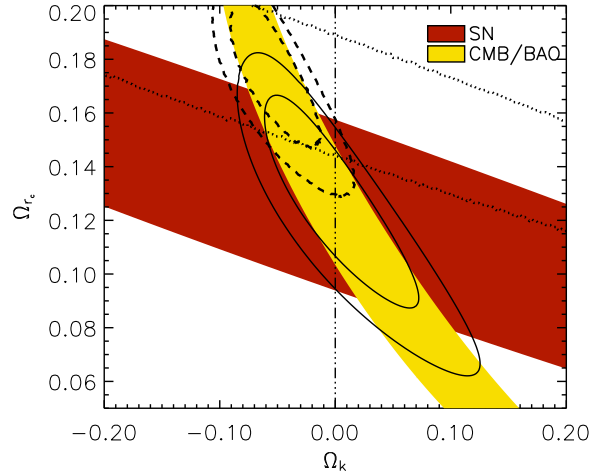$$\mathrm{AIC} = -2\ln\mathcal{L} + 2k, \quad (10)$$

Fig. 2.— The constraints from SNe and CMB/BAO on the parameters in the DGP model. The results have changed substantially from those of Davis et al. (2007). This is both due to the new datasets and our choice of not using CMB-$\mathcal{R}$. The flat DGP model is indicated by the vertical dashed-dotted line; for the MLCS fit, it is the best-ranked model by the IC analysis. The SALT-II fit to the SNe is again shown by the dotted contours. The combined constraints using the SALT-II SNe outlined by the dashed contours represent a poorer match to the CMB/BAO for the flat model.

where $\mathcal{L}$ is the maximum likelihood, k is the number of parameters, and N is the number of data points used in the fit. A ΔBIC larger than 6 would be considered unsupported as compared to the best model.

The number of degrees of freedom is derived from the 288 SNe and the two CMB/BAO measurements, less the contribution from $\mathcal{M}$ and the number of parameters listed in Table 1. Note that the fairly low χ^2 per degree of freedom stems from the fact that we add an intrinsic dispersion to the supernova data. As mentioned above, this is derived by measuring the dispersion in the nearby sample. The SDSS SNe actually have a lower dispersion (0.08 mag), which K09 attribute to selection effects (K09, their Appendix E). We also ran a test with this lower intrinsic dispersion, 0.08 mag, and found that while the fits are now much worse (higher χ^2 and very low GoF), the relative ΔAIC are not affected by much. Some rank order differences would be seen in Table 2, but only for differences of ΔIC$\lesssim$1, and these should not be regarded as significant. Since the intrinsic dispersion has somewhat different meaning in the SALT and the MLCS frameworks, it makes little sense to compare the GoF for the different light-curve fitters.

Compared to the analysis performed earlier by D07, we can see that the new MLCS dataset provides different results in several interesting ways, as follows.

- There are now a number of exotic models that fare rather well under the IC test. It is clear that both this dataset and the method we have used to combine the observational constraints permit a larger variety of models. We note in particular that many of the models provide very similar χ^2 values, and the IC tests therefore are sensitive to the number of parameters for the given model.
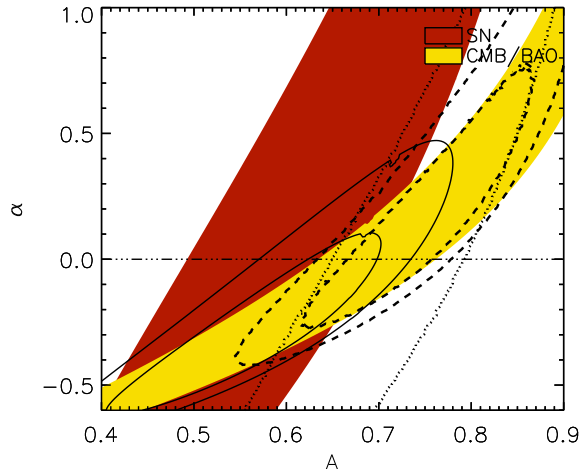
FIG. 3.— Constraints for the flat generalized Chaplygin gas (FGCh). From the constraints in this analysis, this model cannot be excluded. The dashed-dotted $\alpha = 0$ line corresponds to parameters that match the Λ model (with $\Omega_m = 1 - A$), and these do not match the combination with the MLCS fit data. The best MLCS fit is at $\alpha = -0.4$, $A = 0.55$, which is far from the $\alpha = 0.0$, $A = 0.7$ that represents the best fit to the FΛ model. This is different from the analysis of D07 when the best fits were acquired for parameter values that mimic the cosmological constant. The combined constraints from the SALT-II SNe (dashed) are more consistent with FΛ values.

- The simple, flat, cosmological-constant model (FΛ) favored by D07 is no longer on top of the ranking list in Table 2. This can of course be understood from Figure 1. Instead, the model favored by both ΔBIC and ΔAIC is the flat DGP model that was unsupported by previous studies. In Figure 2 we can see the constraints on the DGP model from the new data and analysis. These are very different from the case presented by D07. The change is driven by the new SN data, and is exacerbated by the way we now combine the CMB/BAO and SN constraints (i.e. omitting CMB-$\mathcal{R}$).

- The flat dark-energy model (Fw) may still be a viable model for this new dataset in terms of ΔIC. However, in Figure 1 we see that the most likely value from the combined dataset is $w = -0.83 \pm 0.24$ (95% confidence level [C.L.] for one parameter). For this model, the value of $\Omega_m = 0.31 \pm 0.06$. Including CMB-$\mathcal{R}$ as in Figure 1, which is viable for this model, gives $w = -0.79 \pm 0.13$. This offset from $w = -1$ is clearly a feature of the new MLCS analysis of the combined supernova dataset (see also K09). The more general Fwa model gives the best-fit value of $w_0 = -0.73 \pm 0.38$, while there are no useful constraints on the time varying component of $w(a)$.

- Models such as the generalized Chaplygin gas were found by D07 to be good fits to the data only when their parameters mimicked a cosmological constant. The new best fits instead fall in regions of parameter space that do not correspond to the cosmological constant. This is, for example, shown for the flat generalized Chaplygin gas in Figure 3.

The Cardassian expansion model is not very well

Model	$\chi^2/$ dof	GoF (%)	ΔAIC	ΔBIC	$\Delta\Delta$AIC$_{Rv}$
FDGP	233.3 / 288	99.21	0.0	0.0	-2.3
Λ	233.2 / 287	99.12	1.9	5.6	0.0
DGP	233.2 / 287	99.12	2.0	5.6	0.4
FGCh	233.3 / 287	99.11	2.1	5.7	0.3
Ch	233.4 / 287	99.10	2.1	5.8	-1.7
Fw	233.5 / 287	99.09	2.2	5.9	0.5
Fwa	233.1 / 286	99.03	3.8	11.1	1.9
w	233.2 / 286	99.02	3.9	11.2	1.0
Ca	233.2 / 286	99.02	3.9	11.2	0.7
GCh	233.2 / 286	99.01	3.9	11.3	0.9
FΛ	237.3 / 288	98.70	4.0	4.0	4.0
LTBg	235.5 / 286	98.69	6.2	13.6	4.2
LTBs	237.6 / 286	98.31	8.3	15.7	6.8
FCh	257.6 / 288	90.09	24.3	24.3	13.2

NOTE. — For our SN sample analyzed with MLCS plus CMB/BAO, the FDGP model is preferred by both the AIC and the BIC. The ΔAIC and ΔBIC values for all other models in the table are then measured with respect to these lowest values. The goodness of fit (GoF) approximates the probability of finding a worse fit to the data. The models are given in order of increasing ΔAIC. The final $\Delta\Delta$AIC$_{Rv}$ column simply displays the difference in ranking when using different priors in the MLCS supernova analysis, as described in Section 4.1.1.

constrained but also in this case the best fit does not match the FΛ model. This agrees with the poorer rating of the cosmological-constant model in the present investigation.

- The only model that is very strongly unsupported compared to the other models is the flat Chaplygin gas.

In addition to the contour plots, we provide in Figure 4 a Hubble diagram displaying a selection of the discussed models. This representation offers perhaps a less abstract way to judge the models. Note that the best-fit models are in the upper panel of Figure 4 constrained both by the SNe Ia and the CMB/BAO, i.e., the model parameters are not optimized for a supernova Hubble diagram.

4.1.1. Changing the MLCS Priors

The MLCS light-curve fitter used by K09 is an updated version of the MLCS used by Wood-Vasey et al. (2007, hereafter WV07). The new features include in particular new priors and an updated treatment of extinction. As shown by K09, this new treatment significantly changes the best-fit w value for the Fw model, and this is not a feature of the new SDSS-II SN dataset.

To illustrate how these parameters within MLCS affect our cosmology ranking we have also performed calculations for an alternative set of assumptions. Following the discussion in K09 (their Section 10.1.4 and Fig. 32) we start with the WV07 prior and then implement all of the cumulative changes up to (but not including) the point where K09 also change R_V from the typical Milky Way value of 3.1 to the lower value of $R_V = 2.2$. This is of course a rather arbitrary choice of parameter changes, and is just meant to illustrate how different MLCS assumptions and implementations affect the fits to the Hubble diagram for the models tested in this paper. This particular choice corresponded to an offset in w of $\lesssim 0.1$ for the Nearby+ESSENCE+SNLS dataset analyzed using the Fw model according to K09 (their Fig. 32). We
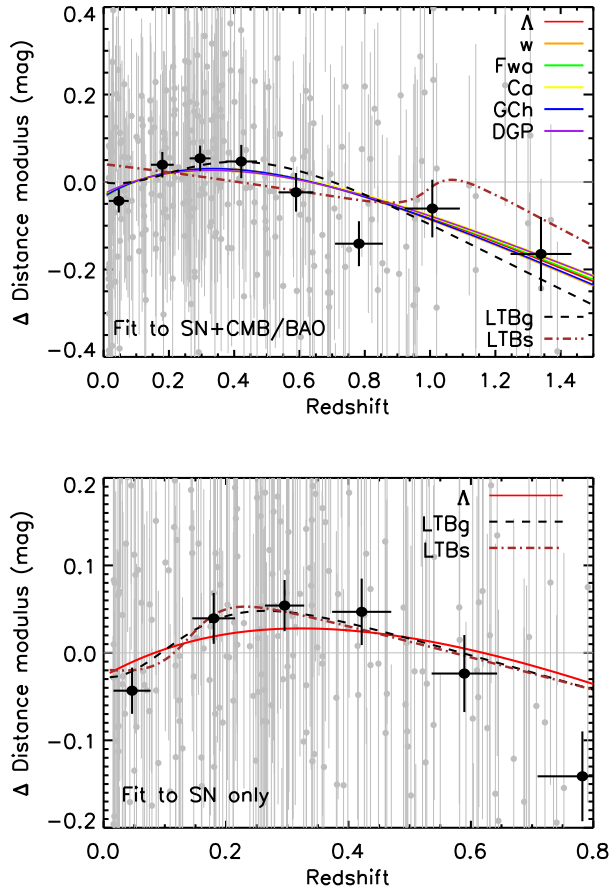
FIG. 4.— (Upper) Hubble diagram for the MLCS supernova analysis. Distance modulus differences in magnitudes are shown with respect to an empty universe. The grey points are the SN Ia distance moduli with error bars, while the black points are binned data. The binning is done using $n\Delta z$=constant, where n is the number of SNe in the bin and Δz the redshift range. This uniform and unbiased binning was introduced by Riess et al. (2007) to enable visualizing the Hubble diagram with bins distributed over the entire redshift range, and with $n\Delta z = 6$ we get 8 bins with error bars that are of similar size in both directions. The redshift error bars show the standard deviation of the redshifts in the bin, while the distance modulus error bars give the standard deviation of the mean of the distance modulus uncertainties within the bin. Note that the binning is only used for visualization in this figure, and that all the calculations and fits are performed on the unbinned data. We have also plotted the best fits for a sample of models (we chose mainly the non-flat models in order not to clutter the figure). In the upper panel, these best fits are using MLCS SNe and the CMB/BAO constraints, i.e., they are not optimized for the SN Hubble diagram alone. In order to plot these Hubble diagrams, the best fit value has been used for the different models. For example, for the upper panel and the Λ model we derived $\mathcal{M}$-$M = 5\log(c/H_0) + 25 = 43.35$. Here, c is the speed of light, H_0 the Hubble constant (where (c/H_0) is in Mpc) and M is the absolute magnitude of a Type Ia supernova. The other models included in the figure have similar values for $\mathcal{M}$ ($\sigma = 0.02$ mag), with the LTBs model having the largest offset. Note that in all the calculations, these nuisance parameters were marginalized over. (Lower) Hubble diagram for the best fits to the MLCS SN Ia data alone, relative to an empty universe. This panel is zoomed in to focus on the sharp LTB (dotted) and the Gaussian LTB (dot-dashed) models. For comparison we have also plotted the best-fit Λ model.

perform here the calculations for all of our exotic models, for our choice of CMB/BAO prior, and for the complete SN dataset used in our analysis.

The results of the different assumptions in the MLCS are given as the $\Delta\Delta\mathrm{AIC}_{Rv}$ values in the last column of Table 2. This is simply the differences in $\Delta\mathrm{AIC}$ compared to our original MLCS analysis, i.e., $\Delta\Delta\mathrm{AIC}_{Rv} = \Delta\mathrm{AIC}_{\mathrm{MLCS}} - \Delta\mathrm{AIC}_{\mathrm{new\,priors}}$, with both runs normalized to the best-fit model. To not overload the presentation, we have chosen to include only the AIC statistics here, since this is an asymptotically unbiased estimator (Burnhamn & Anderson 2004). The differences are not very large in this representation. Note again that differences of $\lesssim 1$ in $\Delta\mathrm{IC}$ are not significant. All models fare slightly better compared to the FDGP model in this case. A noticeable difference is that the FΛ model fares significantly better using this set of MLCS priors. In the Fw model, $w = -0.99 \pm 0.28$. We stress that we in no way prefer this set of parameters, but use them only to illustrate how such changes would affect our model selection.

4.2. LTB

Here we take the opportunity to further discuss the results of our LTB models. Combining the SN data with the CMB/BAO constraint provides a critical test of the validity of our LTB models, since there appears to be some tension between the best-fit parameter values preferred using the SNe and CMB/BAO data separately. This of course assumes that the BAO constraints can be used in this way also for LTB models (see Garcia-Bellido & Haugbølle 2008). The total χ^2 values for our LTB fits are comparable to those of the other models (Table 2), and because of the extra parameters the LTB models fare poorly in the IC tests. These conclusions generally agree with what Garcia-Bellido & Haugbølle (2008) found for their LTB models.

Our best-fit models (using the MLCS supernova analysis) show the transition, r_0, at 1.2 (1.8) Gpc h^{-1} for the LTBg (LTBs) models. For the LTBg the matter density $\Omega_{\mathrm{in}} = 0.25$, $\Omega_{\mathrm{out}} = 0.72$, and these numbers are similar for the LTBs model. This is illustrated in Figure 5.

We note that some of the LTB models studied in the literature display distinct features in the low-z end of the Hubble diagram (e.g., Alexander et al. 2007; Clifton et al. 2008). It was therefore anticipated that the SDSS-II data would provide decisive constraints by filling in the redshifts desert between $z \approx 0.1$ and $z \approx 0.4$. The smooth Hubble diagram in this redshift regime provided by our well-calibrated SDSS-II supernova dataset (see K09, their Fig. 23) clearly disfavors such luminosity distance vs. redshift relations.

However, not all LTB models investigated possess such conspicuous features (Alnes et al. 2006; Garcia-Bellido & Haugbølle 2008). In fact, our simple LTB models can fit the SN data (alone) with a χ^2 somewhat lower than that of the FΛ model. This is illustrated in the Hubble diagrams in Figure 4, where the LTB models are included together with a selection of other alternative models. In the upper panel Hubble diagram all models have also been constrained by the CMB/BAO data. This combination produces a poorer fit for the LTB models and pushes the transition to higher redshifts. The
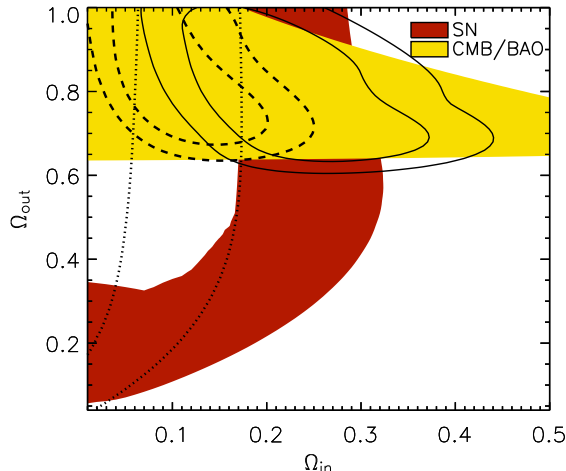
FIG. 5.— The LTB Gauss model is able to give a reasonable fit to the data but is not favored by the IC tests. It is clear that the data prefer the matter density to vary from a low value locally to a higher value in the distant universe. The scale size of the void in the best-fit model is 1.2 Gpc/h. The SALT-II SNe (dotted) push Ω_{in} to lower values while leaving the constraint on Ω_{out} unchanged.

lower panel instead displays the LTB Hubble diagram when fit only to the supernova data, and demonstrates that a good fit to the data can be obtained.

The more general conclusion of our LTB model test is therefore that the SDSS-II SN set is useful for testing the LTB models, but perhaps not decisive to the degree previously anticipated. Although the SDSS-II supernova set strongly constrains LTB models that display egregious features in the intermediate-redshift Hubble diagram, versions of the LTB model that do not display such features, such as the LTBg and LTBs models considered here, can be made to fit the supernova data.

However, in terms of our IC test, we have found that these LTB models are not well motivated; the number of extra parameters involved is not justified by a better fit to the SN data, in particular not when the CMB/BAO constraints are also included. Note that these results also hold when using the SALT-II light-curve fitter to analyze the SN data (Table 3). We also mention that if we were to impose the prior of asymptotic flatness on our LTB models, the χ^2 for these fits would increase even further.

4.3. Model Ranking Using the SALT-II Analysis

We have also performed calculations using SN data fit with the completely independent light-curve fitter SALT-II (Guy et al. 2007), following the implementation as described by K09. K09 noted a substantial offset for the value of w as calculated in the standard model using MLCS versus SALT-II, and devote a long discussion to the differences of these light-curve fitters. As seen in Figure 1, the SALT-II fits are more consistent with the concordance model, and we here investigate in detail how such a difference alters our ranking of the investigated exotic models.

In performing these calculations, we had to exclude four of the SNe that were well fit by MLCS because in the SALT-II analysis they gave poor fits[24].

[24] The SNe designated d085, e020, k429, and HAWK.

The SALT-II prescription clearly makes the SN data more compatible with the standard models. In Table 3 we see that the highest-ranked model is the FΛ model, a flat universe with a cosmological constant. It has a similar χ^2 as many of the other models, and is primarily favored by the IC since it has only one free parameter. This echoes the conclusions of D07. In the rightmost column of Table 3 we provide the difference in ΔAIC compared to the MLCS results, to illustrate which models benefit most from using the SALT-II SN set. Note that the numbers of degrees of freedom are less than for the MLCS table both since we had to exclude four SNe, and due to the two extra free parameters in the SALT-II fits. We note the following:

- FΛ evidently fares much better with SALT-II than with MLCS, as was already evident from Figure 1. For the Fw model the best-fit value for the equation-of-state parameter is $w = -1.14 \pm 0.26$ (95% C.L. for one parameter), with $\Omega_m = 0.30 \pm 0.05$. Including CMB-$\mathcal{R}$ as in Figure 1, which is viable for this model, gives $w = -0.98 \pm 0.14$.

- On the contrary, the FDGP model is now pushed toward the bottom of the ranking list. Figure 2 again illustrates the situation, with the SALT-II SN constraint dragging the solution along the CMB/BAO constraint and away from the flat universe. The non-flat DGP model is still one of the models that fares better in this investigation than in D07 (as is the Ch model).

- The LTB models fare as poorly (or worse) compared to the best-ranked models when the SALT-II SN data are used. In this respect the conclusions from Section 4.2 hold independent of the adopted light-curve fitter.

- The SN distances obtained using the SALT-II light-curve fitter provide results that are overall more consistent with the analysis of D07. For the FGCh model (Figure 3), we can see that the SALT-II SN distances allow a match to the CMB/BAO constraints for parameter values that are more consistent with those expected for the cosmological-constant model.

5. SYSTEMATICS

When performing the same kind of IC ranking of cosmological models as in D07, the new datasets and methods explored in this paper lead us to quite different conclusions. When we use the MLCS analysis the standard cosmological-constant model no longer stands out as the best and simplest model, and new room is made for a range of more exotic models. The results from the SALT-II analysis are quite different.

A basic underlying assumption in the analysis is that the errors are mainly statistical. The systematic errors in, for example, the SN surveys are extensively discussed elsewhere (e.g., Astier et al. 2006; Wood-Vasey et al. 2007; Kessler et al. 2009), and the uncertainties include, in particular, the distribution of host-galaxy extinctions (A_V) and the dust-reddening properties (R_V).

While model selection techniques are not well equipped to face systematic errors, we can regard the above-mentioned calculations as a simplistic perturbation theory approach to test how assumptions regarding light-curve fitters affect the model selection.

In Table 2 we illustrate how the model selection is affected by rather arbitrarily changing the priors in the MLCS light-curve fitter. Given the change in results engendered by using the ratio of total-to-selective absorption of $R_V = 2.2$ that K09 derived from the SN sample itself, such a low value of R_V should clearly find support also from independent astrophysical observations.

The most dramatic differences noted in this investigation come from the very different results obtained for the two light-curve fitters investigated. This clearly points to unresolved systematic differences that need to be further explored. Table 3 shows in the final column that the fits of some exotic models are dramatically affected by the choice of light-curve fitter in the analysis of the SN data.

While we acknowledge the way Kowalski et al. (2008) treat the SN data from their large Union08 compilation, we also note that adding a dispersion to the error mimics the use of more free parameters in the fit. Using the same Union08 dataset, Rubin et al. (2009) reached conclusions similar to the ones in this paper; the difference in χ^2 values for different cosmological models are rather small. We have not included any systematic errors in our tests, and including larger systematic errors would clearly make it even more difficult to differentiate between cosmological models for a given dataset.

However, it is also clear from our investigation that trying to encapsulate the systematic errors is notoriously difficult. The substantial disagreement in model selection obtained with different light-curve fitters investigated here demonstrates that deeper understanding of the systematics is warranted. It is also important to refrain from simply choosing the method or datasets that confirm previous findings or present prejudices.

6. GENERAL EXPANSION HISTORY

Given the difficulty in assessing particular models, we also consider some ways to derive more general cosmological results from our dataset. The usual parameter-fitting techniques used in cosmology are limited by the necessity of assuming a model with parameters to fit; there is more information in the cosmological data than can be extracted by parameter fitting. In this section we will ignore specific dark energy theories and instead try to elucidate directly the expansion history of the universe, $H(z)$, or the evolution of an equation-of-state parameter of dark energy, $w(z)$. The SN dataset fitted with MLCS is used here, since this easily provides distance moduli without having to fit a specified cosmology for the $H(z)$ section, and it avoids additional free parameters for the $w(z)$ analysis.

6.1. *The Equation-of-State Parameter $w(z)$*

We start this investigation by assuming a piecewise constant equation-of-state parameter, in order to fit a more general dark-energy model. The value w_i is calculated in each redshift bin i (defined by the upper limit z_i), where we have arbitrarily chosen $z_i = [0.15, 0.6, 1.7, 1090]$, roughly corresponding to low-, mid-,

TABLE 3
INFORMATION-CRITERIA RESULTS FOR SALT-II

Model	χ^2/ dof	GoF (%)	ΔAIC	ΔBIC	$\Delta\Delta$AIC$_{\mathrm{MLCS}}$
FΛ	274.4 / 282	61.63	0.0	0.0	4.0
FGCh	273.0 / 281	62.32	0.6	4.3	1.5
Λ	273.4 / 281	61.66	1.0	4.6	0.9
DGP	273.4 / 281	61.65	1.0	4.7	1.0
Ch	273.9 / 281	60.87	1.5	5.1	0.7
Fw	274.0 / 281	60.67	1.6	5.3	0.6
GCh	273.0 / 280	60.61	2.6	10.0	1.3
Fwa	273.4 / 280	60.05	3.0	10.3	0.8
Ca	273.4 / 280	59.97	3.0	10.3	0.9
w	273.5 / 280	59.82	3.1	10.4	0.8
LTBg	276.5 / 280	54.71	6.2	13.5	0.0
FCh	281.9 / 282	49.06	7.5	7.5	16.8
FDGP	282.5 / 282	48.05	8.1	8.1	−8.1
LTBs	289.3 / 280	33.90	18.9	26.2	−10.6

NOTE. — For our SN sample analyzed with SALT-II plus CMB/BAO, the FΛ model is preferred by both the AIC and the BIC. The ΔAIC and ΔBIC values for all other models in the table are then measured with respect to these lowest values. The goodness of fit (GoF) approximates the probability of finding a worse fit to the data. The models are given in order of increasing ΔAIC. The numbers of degrees of freedom are less than for the MLCS fits, since four SNe were omitted and because SALT-II uses two extra fit parameters. The final column simply displays the AIC differences as compared to the MLCS results in Table 2, i.e., $\Delta\Delta$AIC$_{\mathrm{MLCS}}$=ΔAIC$_{\mathrm{MLCS}}$−ΔAIC$_{\mathrm{SALT}}$.

high-z SNe and CMB data, respectively. We have fitted both w_i and Ω_m using a Monte Carlo Markov Chain, assuming a flat universe.

Note that the w_i are correlated; the covariance matrix is not diagonal. We can, however, decorrelate the w_i estimates by (following Huterer & Cooray 2005) changing the basis through an orthogonal matrix rotation that diagonalizes the covariance matrix. This corresponds to applying a weighting function to the w_i. The uncorrelated w_i are thus linear combinations of all w_i described by the weight function.

That is, appropriately weighted data from all redshifts are used to obtain w in each bin, and in our case, the value of w_i corresponding to low redshifts (w_1) is a linear combination of the value of $w(z)$ at $z < 0.15$ ($\sim 82\%$ contribution), $w(0.15 < z < 0.6)$ ($\sim 18\%$ contribution), and negligible contributions from higher redshifts. In the same way, w_2 is a combination of $w(z < 0.15)$ ($\sim 24\%$ contribution), $w(0.15 < z < 0.6)$ ($\sim 73\%$ contribution) and $w(0.6 < z < 1.7)$ ($\sim 3\%$ contribution). The value of w_3 has a $\sim 17\%$ contribution from $w(0.15 < z < 0.6)$ and a $\sim 87\%$ contribution from $w(0.6 < z < 1.7)$, whereas w_4 predominantly comes from the highest redshift bin and only has small negative contributions from the three lower redshift bins.

The results are presented in Figure 6, and are discussed in Section 6.4.

6.2. *The Hubble Parameter $H(z)$*

Wang & Tegmark (2005) proposed a technique to extract the expansion history in uncorrelated redshift bins from SNe Ia data. This technique was used to great effect by Riess et al. (2007). We now apply it with the new information from the SDSS-II supernova sample.

The results are displayed in Figure 7, where the theoretical models have been normalized as described in the caption. The redshift bins have been chosen by the requirement that the ratio of the error on the Hubble pa-
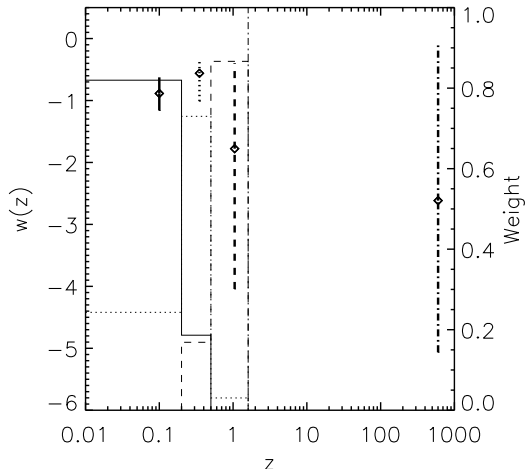
FIG. 6.— Observational constraints on a piecewise constant $w(z)$ plotted (diamonds) at the middle value in each redshift bin. Note here that results are given not in terms of the original $w(z)$ but weighted with data from all redshift bins in order to decorrelate the bins. The weights are displayed as thin lines with styles corresponding to the respective points, and with the scale given on the right-hand side of the figure. This is further detailed in the text (Section 6.1). The results include our CMB/BAO constraints. The error bars are 68%. The constraints on the evolution of $w(z)$ at $z \gtrsim 1$ are clearly very weak.

rameter and the redshift range probed by each measurement should be close to a constant times the redshift derivative of the Hubble parameter; we want to keep a uniform signal-to-noise ratio across the bins. Ideally, this constant should be equal to one, corresponding to

$$\sigma_H = \frac{dH}{dz}\Delta_z \ , \qquad (11)$$

where σ_H is the uncertainty in the Hubble parameter and Δ_z is the redshift range that each measurement probes, as calculated by Wang & Tegmark (2005). We compute dH/dz using a fiducial cosmological model, here taken to be a flat universe with $\Omega_m = 0.3$.

We find that when using three redshift bins, the error from the width of the redshift bin dominates, whereas for four bins, the Hubble parameter uncertainty is somewhat larger than the corresponding error from the redshift range probed. Note that only the supernova data are used in obtaining $H(z)$.

6.3. *The Deceleration Parameter q*

Another less theory-dependent investigation comes from exploring the deceleration parameter and its evolution. Following Mörtsell & Clarkson (2009), we consider a flat universe where

$$q(a) = q_0 + q_1(1-a) = q_0 + q_1 \frac{z}{1+z} \ . \qquad (12)$$

At zero redshift, $q(a = 1) = q_0$ and in the infinite past, $q(a = 0) = q_0 + q_1$. This parametrization appears to be reasonably flexible in the sense that performing a least-squares fit to the dark-energy models employed in this paper always provides an acceptable fit. The comoving distance is given by

$$d_c(z) = \int_0^z \frac{dz}{H(z)} = \frac{1}{H_0} \int_0^z \exp\left[-\int_0^v \frac{[1+q(u)]du}{(1+u)}\right] dv \ , \qquad (13)$$
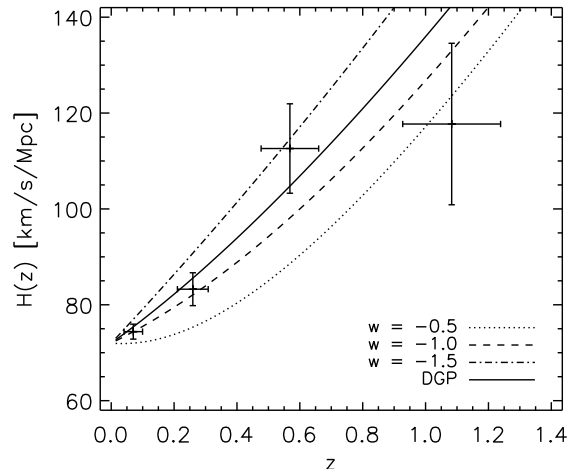
FIG. 7.— With the rich SN dataset we can also trace $H(z)$ in a more model-independent way. Here the $H(z)$ evolution is compared to some theoretical models. The models are normalized to agree at redshift zero, and we have assumed $H_0 = 72$ km s^{-1}Mpc^{-1}. The data points are normalized to have the lowest-redshift bin on the $w = -1$ curve, and the four different points are independent of each other. Only supernova data were used for this plot, and a flat universe was assumed.
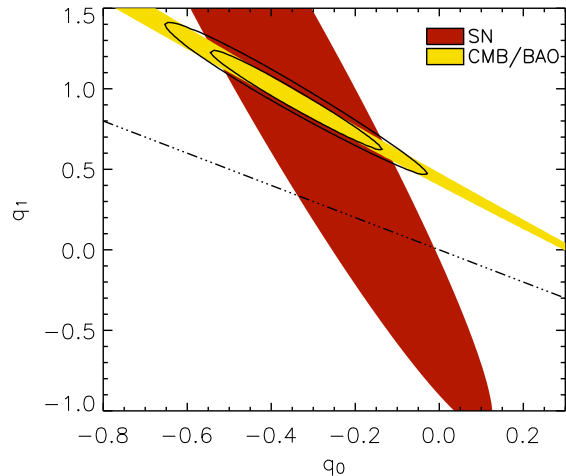
FIG. 8.— Another less model-dependent investigation comes from exploring the deceleration parameter and its evolution. Following Mörtsell & Clarkson (2009), we plot this representation together with our new observational constraints. On the abscissa, the evidence for current acceleration is evident. The dashed-dotted line demarcates models with early deceleration (above the line) from model with early acceleration; that the best-fit lies well above this line demonstrates evidence for past deceleration.

and the luminosity distance, which is the relevant quantity for SN Ia observations, is given by

$$d_L(z) = \frac{1+z}{H_0\sqrt{|\Omega_k|}} S_k\left[\sqrt{|\Omega_k|}H_0 d_c(z)\right] . \qquad (14)$$

The angular diameter distance, relevant for the scale of BAO and CMB, is given by $d_A = d_L/(1+z)^2$. We can now use Figure 8 to study the expansion history of the universe within this simple flat model, as discussed below.
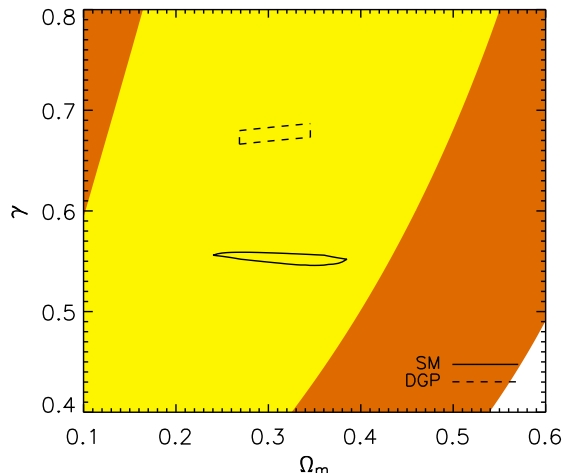
6.4. *General Results*

FIG. 9.— The growth of structure is an independent way to constrain cosmological models. This is illustrated here for standard gravity (SM) and for the DGP model (see Section 6.5). It is clear that the present data do not yet select between these models, but any future deviations from $\gamma = 0.55$ above a few percent would indicate deviations from ordinary gravity. Solid and dashed lines are 95% confidence levels for one parameter while the filled yellow (light) and orange (dark) regions show 68.3% and 95% confidence levels for two parameters respectively.

The method of presenting the evolution of $w(z)$ and $H(z)$ given in Figs. 6 and 7 may have more general and long-lasting value than fits to specific models.

The $H(z)$ evolution shown in Figure 7 is displayed together with a few cosmological models. We can see how the DGP model produces an acceptable fit to the evolution of the Hubble parameter. The general trend, an increasing value for $H(z)$ with increasing redshift, is clear.

Any $w(z)$ evolution would be an obvious signature of exotic models. We do not, however, see any statistically significant evolution of w in Figure 6 (see also Kowalski et al. 2008). This representation could also be used to constrain generic "freezing" and "thawing" models, following, e.g., Sullivan et al. (2007); Caldwell & Linder (2007), and in this respect Figure 6 can be seen as an illustration of our ability to model-independently constrain the evolution of w using current data. We note that the result that w is consistent with -1 across the redshift range does not depend on the choice of binning, although the size of the error bars does. Using Eq. 11 we derive for our combined SNe Ia and CMB/BAO constraints (Figure 8) $q_0 = -0.34 \pm 0.16$ and $q_1 = 0.93 \pm 0.25$. The negative value of q_0 demonstrates that the present universe is accelerating. Note, however, that with the current (MLCS) dataset, this conclusion does not follow for this parametrization for the SN dataset alone. Furthermore, the fact that the combined contour clearly hovers above the dashed-dotted line demonstrates that the universe was also decelerating in the past. The redshift where the universe transits from a decelerated expansion to an accelerated expansion is constrained to $0.41 < z_t < 0.72$ (95% C.L. for one parameter).

6.5. Growth Factor, γ

There are a number of more exotic models that cannot be ruled out, even in principle, if the magnitude-redshift

evolution we observe remains consistent with ΛCDM. This is because they can mimic standard dark energy perfectly in this respect.

For many of these models, it would be useful to investigate additional and complementary constraints that can distinguish them from ΛCDM. This can be done using information about structure formation as expressed by the growth factor (Linder 2005; Linder & Cahn 2007). It is a measurable parameter of a model, in the same sense as the matter density Ω_m or the equation-of-state parameter w. All models in which general relativity holds have a growth parameter $\gamma \approx 0.55$, but models that explain the acceleration by modifying gravity may have a significantly different growth factor. Thus, this approach has the potential to separate models that have identical predictions for expansion history but differ in the form of gravity.

We show in Figure 9 the predicted growth factor for the DGP model and for the standard model (SM=Fw, dashed and solid contours, respectively), together with constraints from current data (filled contours). The DGP model has the same number of parameters as the cosmological-constant model, and can therefore provide a useful framework for testing modified gravity alternatives. The DGP model fared very well in the IC test in Table 2, but does give different predictions for the growth of structure.

Figure 9 uses the new data from Guzzo et al. (2008) analyzed following the procedure of Linder & Cahn (2007). The filled contours are growth-factor data ($f \propto \Omega_m^\gamma$) using $f = 0.49 \pm 0.14$ at $z = 0.15$ and $f = 0.91 \pm 0.36$ at $z = 0.77$. It is clear that the present data do not yet select between these models, but any deviations from $\gamma = 0.55$ above a few percent would indicate departures from ordinary gravity.

7. CONCLUSIONS

We have followed the information-criteria model selection outlined in D07 using the new supernova dataset from the SDSS-II (K09) and a new way to combine the updated BAO and CMB datasets. The ranking using the MLCS supernova analysis is quite different from the models selected by D07, with more room for exotic models. Using instead the SALT-II light-curve fitter, we obtained fits more consistent with the cosmological constant. Some LTB models were also tested; they were able to give decent fits to the SN data, but were not favored by the full IC tests.

We also discuss how more general results can be derived from this new dataset, and demonstrate that the expansion of the universe is indeed speeding up now, while it used to be slowing down. This conclusion is based on combining constraints from the supernova data with complementary data.

The information-criteria tests used in this analysis are fairly simple, but serve the purpose to quantitatively rank models with rather similar χ^2-fit values. The way the results differ between the different light-curve fitters suggests that more detailed statistical tests are not justified.

The data from the releases of several major supernova searches (SDSS-II, ESSENCE, SNLS, *HST*) have been analyzed in this paper. Most of these teams plan to release substantial updates of their supernova samples

soon. This will be important in improving the statistics, but our analysis also makes clear that systematic effects, in particular uncertainties in the treatment of extinction and light-curve fitting, will limit the predictive power in selecting a model based on these data. Rather than determining w with increased accuracy, sometimes claimed to be measured to within $\sim 6\%$ (e.g., Kowalski et al. 2008; Komatsu et al. 2009), this work cautions on the importance of the systematic effects.

We note that the recent investigation by Hicken et al. (2009) also finds differences in the derived value for w using different light-curve fitters and also for different cuts in the datasets, and provide several good suggestions on how to improve future supernova cosmology in this regard. The SDSS-II dataset is indeed of sufficiently high quality to enable further studies of the relevant systematics.

We have explored how systematics limit our ability to select the best models for the universal expansion based on current data. A discussion on the benefits of MLCS versus SALT-II is beyond the scope of this paper. K09 trace part of the discrepancies to the way the light-curve fitters treat extinction, how this affects very blue SNe and in particular to uncertainties in the bluest pass-bands. Better constraints on the systematics from the final data releases from SDSS-II, ESSENCE, and SNLS may well help in resolving some of the tension discussed in this paper. We may then find that our standard model holds. Or we may simply live in a more exotic universe.

ACKNOWLEDGMENTS

REFERENCES

Alnes, H., Amarzguioui, M., & Grøn, Ø. 2006, Phys. Rev. D, 73, 083519
Alexander, S., Biswas, T., Notari, A., & Vaid, D. 2007, ArXiv e-prints, 712, arXiv:0712.0370
Astier, P., et al. 2006, A&A, 447, 31
Bondi, H. 1947, MNRAS, 107, 410
Burnham, K. P., & Anderson, D. R., 2004, Sociological Methods Research, 33, 261
Caldwell, R. R., & Linder, E. V. 2007, Phys. Rev. Lett., 95, 141301
Caldwell, R. R., & Stebbins, A. 2008, Phys. Rev. Lett., 100, 191302
Clifton, T., Ferreira, P. G. & Land, K., 2008, Physical Review Letters, 101, 131302
Davis, T. M., et al. 2007, ApJ, 666, 716 (D07)
Elgarøy, Ø., & Multamäki, T. 2007, A&A, 471, 65

Enqvist, K., & Mattsson, T. 2007, Journal of Cosmology and Astro-Particle Physics, 2, 19
Filippenko A. V., 2005, in White Dwarfs: Cosmological and Galactic Probes, ed. E. M. Sion, S. Vennes, & H. L. Shipman (Dordrecht: Springer), 97
Frieman, J. A., et al. 2008, AJ, 135, 338
Garcia-Bellido, J., & Haugbølle, T. 2008, Journal of Cosmology and Astro-Particle Physics, 4, 3
Gunn, J. E., et al. 2006, AJ, 131, 2332
Guy, J., et al. 2007, A&A, 466, 11
Guzzo, L., et al. 2008, Nature, 451, 541
Hicken, M., et al. 2009, ApJ, 700, 1097
Huterer, D., & Cooray, A. 2005, Phys. Rev. D, 71, 023506
Jha, S., Riess, A. G., & Kirshner, R. P. 2007, ApJ, 659, 122
Kessler, R., et al. 2009, ApJS in press, astro-ph, 0908.4274 (K09)
Komatsu, E., et al. 2009, ApJS, 180, 330

Kowalski, M., et al. 2008, ApJ, 686, 749
Kurek, A., & Szydłowski, M. 2008, ApJ, 675, 1
Lampeitl, H., et al. 2009, submitted to MNRAS
Lemaître, G. A. 1933, Ann. Soc. Sci. Brux. 53, 51
———— 1997, General Relativity and Gravitation, 29, 641
Liddle, A. R. 2004, MNRAS, 351, L49
Linder, E. V. 2005, Phys. Rev. D, 72, 043529
Linder, E. V., & Cahn, R. N. 2007, Astroparticle Physics, 28, 481
Mörtsell, E., & Clarksson, C. 2009, JCAP, 1, 44
Percival, W. J., et al. 2007, ApJ, 657, 51
Percival, W. J., et al. 2009, astro-ph, 0907.1660
Perlmutter, S. et al. 1999, ApJ, 517, 565
Riess, A. G., et al. 1998, AJ, 116, 1009

Riess, A. G., et al. 2004, ApJ, 607, 665
——. 2007, ApJ, 659, 98
Rubin, D., et al. 2009, ApJ, 695, 391
Sako, M., et al. 2008, AJ, 135, 348
Sullivan, S., Cooray, A., & Holz, D. E. 2007, Journal of Cosmology and Astro-Particle Physics, 9, 4
Tolman, R. C. 1934, Proceedings of the National Academy of Science, 20, 169
Wang, Y., & Mukherjee, P. 2006, ApJ, 650, 1
Wang, Y., & Tegmark, M. 2005, Phys. Rev. D, 71, 103513
Wood-Vasey, W. M., et al. 2007, ApJ, 666, 694 (WV07)